ELSEVIER

Journal of Nuclear Materials 317 (2003) 32–45

journal of nuclear materials

www.elsevier.com/locate/jnucmat

Influence of irradiation temperature and dose gradients on the microstructural evolution in neutron-irradiated 316SS

D.J. Edwards *, E.P. Simonen, F.A. Garner, L.R. Greenwood, B.M. Oliver, S.M. Bruemmer

Materials Interfaces and Characterization Group, Pacific Northwest National Laboratory, Structural Materials Development, MSIN P8-15, Richland, WA 99352, USA

Received 20 February 2002; accepted 26 November 2002

Abstract

A cold worked 316SS baffle bolt was extracted from the Tihange pressurized water reactor and sectioned at three different positions. The temperature and dose at the 1-mm bolt head position were 593 K and 19.5 dpa respectively, whereas at two shank positions the temperature and dose was 616 K and 12.2 dpa at the 25-mm position and 606 K and 7.5 dpa at the 55-mm position. Microstructural characterization revealed that small faulted dislocation loops and cavities were visible at each position, but the cavities were most prominent at the two shank positions. Measurable swelling exists in the shank portions of this particular bolt, and accompanying this swelling is the retention of very high levels of hydrogen absorbed from the environment. The observation of cavities in the CW 316SS at temperatures and doses relevant to LWR conditions has important implications for pressurized water reactors since SA 304SS plates surround the bolts, a steel that usually swells earlier due to its lower incubation period for swelling.

1. Introduction

Cracking of both replaceable and non-replaceable components in the core of light water reactors (LWR) continues to be an important issue for the nuclear industry. Examples of replaceable components include instrument tubes, springs, bolts, guides and fasteners, whereas core shrouds and the upper guide structures represent examples of non-replaceable components that have experienced cracking. Much of the cracking is environmentally-induced by a process known as irradiation-assisted stress corrosion cracking (IASCC), which has recently been reviewed by Bruemmer et al. [1]. IASCC occurs in both boiling water and pressurized water reactors (BWR and PWR, respectively) at irradiation temperatures typically around 561 K, and in certain locations outside the reactor core can extend up to 643 K. Outside the reactor core, substantial gradients in the temperature and dose rate occur over just a few centimeters. The microstructural evolution and the concomitant changes in mechanical and physical properties are not well understood under these irradiation conditions, particularly in relation to how they affect IASCC susceptibility.

The baffle-former plate structure in the core of PWRs is an example of a structure where significant gradients exist in the neutron dose rate and irradiation temperature. These plates are either welded or bolted together depending on the reactor type, and the bolted structures have been found to exhibit cracking after being in reactor for several years. Cracking of the bolts in these structures was first detected in French CPO series plants by non-destructive examination in 1989 [2,3] and later in the Tihange 1 plant [4]. The inspections of the Tihange 1 baffle bolts between 1991 and 1995 revealed a significant increase in positive indications of cracks [4,5]. This led to a decision to replace 90 bolts with reportable ultrasonic

* Corresponding author. Tel.: +1-509 376 4867; fax: +1-509 376 0418.

E-mail address: dan.edwards@pnl.gov (D.J. Edwards).

0022-3115/03/$ - see front matter
doi:10.1016/S0022-3115(03)00003-5

indications as well as some with inconclusive ultrasonic indications in 1995. A small number of these extracted bolts were retained for metallographic examination and other tests. The cracks in these bolts occurred at the junction between the head and shank positions.

The focus of this paper is the characterization of a bolt removed from the Tihange 1 plant in 1995. This bolt, identified as 2K1R5, was removed from the mid-plane of the former at level 5. Although there was an ultrasonic indication, no cracks were found in this particular bolt during visual examination. The following sections present the details of the microstructure, microchemistry, transmutation and hardness evaluation along the length of the baffle bolt, preliminary results from which were reported earlier by Edwards and co-workers [6]. The irradiation conditions (temperature and dose rate) vary considerably over the length of the bolt, producing different microstructures that highlight the sensitivity to the irradiation conditions. The results will be compared to previous work by Edwards and co-workers [7,8] documenting the microstructural evolution in 304 and 316SS irradiated at 560 K in a BWR.

2. Experimental details

The baffle-former bolts of Tihange 1 were fabricated from a single heat of cold-worked 316SS with a yield strength of 513 MPa, ultimate tensile strength of 670 MPa, and 34% total elongation. The chemical composition of this heat is shown in Table 1. Installation of the baffle-former bolts was carried out to a specified torque, each bolt being tightened, then relaxed and finally tightened again. This procedure leads to baffle-bolt preloads ranging between ~20 and 37.5 kN after taking into account the effects of stress relaxation arising from primary creep occurring during the first rise in temperature to the operating value [5].

The three positions examined for bolt 2K1R5 are shown in Fig. 1. Based on neutronics calculations for the full plant history on a nominally comparable bolt, the estimated doses experienced by the 2K1R5 bolt head were ~19.2, 12.2 dpa at the 25-mm position and 8.5 dpa at the 55-mm position as measured from head of the bolt. Such calculations are considered to be most accurate for positions closest to the reactor core, with less confidence expected for positions away from the bolt head.

An independent experimental assessment of the neutron flux-spectra and dpa levels for this particular bolt was obtained from a process called retrospective dosimetry. In this technique levels of radioactivation, transmutation and/or isotopic ratios of various elements in the bolt itself can be used to determine the integrated neutron flux-spectra. In this case it was sufficient to measure the activities of ^{60}Co and ^{54}Mn by gamma spectroscopy at each of the three bolt positions of

Table 1
Bulk composition (wt%) of the Tihange baffle/former bolt as manufactured

Heat	C	Cr	Ni	Si	Mn	S	P	Mo	Cu	Co	N
AA016	0.028	16.70	12.36	0.72	1.89	0.018	0.020	2.64	–	0.080	0.042

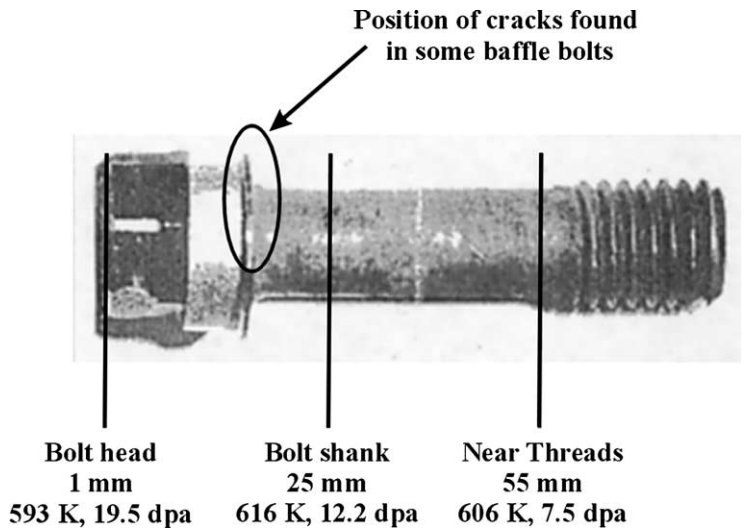

Fig. 1. Three different positions were examined along the length of the bolt. Cracks were found to occur at the junction between the head and shank in some bolts.

interest, as well as the ^{4}He content by isotopic dilution mass spectrometry. Energy dispersive X-ray fluorescence (EDXRF) measurements were also required to measure the Fe content and residual Co content of each specimen since the exact post-irradiation composition of the bolt must be known for confident prediction. A detailed description of the retrospective dosimetry method is provided in reference [9] by Garner and coworkers.

The thermal neutron fluence is proportional to the ^{60}Co produced from the ^{59}Co (n,γ) reaction, and the fast neutron fluence will be proportional to the ^{54}Fe (n,p) reaction. The ratio ^{60}Co/^{54}Mn is therefore proportional to the thermal-to-fast neutron ratio, but this ratio is very time-dependent because both isotopes are decaying continuously, but at different rates. When the detailed power history of Tihange was used to correct the measured activities to saturated reaction rates at the time of removal from the reactor, a completely independent estimate of neutron exposure was determined. One advantage of this technique is that the relative dose experienced by different positions on the bolt is very accurately determined, since all positions on the bolt had exactly the same residence time in reactor and identical decay history. The retrospective technique yielded 19.5 dpa for the 1-mm position, in excellent agreement with the calculated value of 19.2. The retrospective technique shows that the dose falls off somewhat faster with distance along the bolt compared to that predicted by the calculations, being 7.5 dpa compared to 8.7 dpa calculated for the 55 mm position. The dose estimates from the retrospective dosimetry are used throughout the rest of the paper and are listed in Fig. 1.

Indicated temperatures are estimates from a similar bolt position in a French CPO plant at mid-cycle with 600 appm boron remaining in the water. The bolt temperature increased throughout the cycle as the boron was depleted from the water, increasing the thermal neutron population toward the end of the cycle and thereby increasing the local gamma heating rate. The 25-mm position corresponds to the calculated peak temperature position along the length of the bolt. Taking the gamma heating variation into account over the entire cycle, the temperature at the 25-mm position is estimated to increase from 605 to 627 K each reactor cycle.

The microstructure was characterized by performing scanning electron microscopy (SEM) and transmission electron microscopy (TEM) on 3-mm disks punched from slices obtained from the regions indicated in Fig. 1. TEM specimens were electropolished using a 5% perchloric electrolyte in methanol cooled to 233 K. Stringers of sulfide and oxide particles led to specimen preparation problems because numerous small holes formed where inclusions dropped out. This was a particular problem at the 1-mm position. In an attempt to improve the specimen quality, these specimens were further thinned by ion milling to enlarge the thin area. This yielded thin areas for microstructural characterization, but no grain boundaries of suitable orientation were found in the 1-mm position for microchemical analysis. The 25- and 55-mm positions responded better to the electropolishing, but these samples also required ion milling to increase the thin area.

A JEOL 2010F and a JEOL 2000 were used for the characterization. A JEOL 840 SEM was used for the characterization of the grain size and inclusions in the material. Microchemical analyses at internal interfaces, primarily high-angle grain boundaries, were carried out using the JEOL 2010F field emission gun TEM. The microchemical analysis data were obtained from energy dispersive X-ray spectroscopy (EDS) using a high-efficiency link analyzer and detector. A minimum of two grain boundaries was analyzed for each material with multiple measurements on each boundary. Complete compositional profiles across the boundary into the matrix were recorded out to a distance of ± 5 nm in 0.5–1 nm steps, and to ± 20 nm in larger steps. Specific profile steps were selected to map individual boundaries based on observed composition changes. Matrix compositions in each grain (corresponding to boundaries analyzed) were obtained in both point mode and area mode at a distance of ~ 50 nm from the boundary. Profiles were taken from regions less than 50 nm in thickness. The background from radioactive decay had to be subtracted from each spectra to yield the correct composition. Mn X-rays produced by the decay of the ^{55}Fe activation product precluded accurate compositional analysis of Mn. Profiles were not obtained from the 1-mm bolt head position because grain boundaries of suitable orientation were not found.

Hardness at room temperature was measured on all samples using a Tukon Model 300 microhardness tester at a load of 500 g. All specimens (typically 3-mm discs) were given a consistent metallographic surface preparation to a 6-μm finish using SiC paper.

The He content from the three positions was determined by isotope-dilution mass spectrometry following vaporization in a resistance-heated graphite crucible [10]. Hydrogen release at 1200 °C from separate small pieces of the same specimens used for He analysis was measured as a function of time using a quadrupole mass spectrometer [11]. A minimum of two specimens from each position were analyzed for He and H; for the 25-mm position, four measurements were made for the hydrogen to assess the range of hydrogen content.

3. Results

3.1. Microstructural characterization

SEM showed the general grain microstructure of the Tihange bolt to be essentially identical at each position.

Backscatter electron images revealed an equiaxed grain size ranging from 10–30 μm, with heavy twinning due to the initial cold work. Inclusions were found throughout the bolt in the form of stringers and individual particles in the grain interiors, but no visible grain boundary precipitation was observed. EDS analysis indicated that some of the particles were MnS inclusions whereas others contained predominately Al and O with some Si, Cr, Ti and Mn. Although the number of inclusions was somewhat variable from area to area, the SEM micrographs yielded an estimated volume fraction of 0.005 for these inclusions.

Higher resolution TEM revealed the microstructure contained faulted dislocation loops, cavities and fine-scale precipitation. No grain boundary precipitation or denuding of defects along the grain boundaries was observed at any position. The primary type of dislocation defect that evolved during irradiation was the Frank loop, a faulted dislocation loop lying on the {1 1 1} planes with a Burgers vector $1/3a[1\,1\,1]$. Examples of these loops for each of the three positions are shown in Figs. 2–4, as well as a comparison of the size distributions in Fig. 5. A more detailed discussion of the analysis technique used to image the Frank loops was provided previously by Edwards et al. [7,8]. A summary of the average sizes and densities of the loops is provided in Table 2. The range of densities was similar within experimental error and suggested little difference between the three positions. The size distributions indicated that the Frank loops in the 1-mm position possessed a smaller average size than those measured in the other two positions. Each size distribution was asymmetrical, with a narrow peak around 4–6 nm and a broader tail extending up to 30 nm. The loop size distribution for the 55-mm sample revealed that a secondary peak was present at a diameter of ~16 nm.

Cavities were clearly observed at all positions but their size and density differed considerably. A summary of the cavity characteristics are included in Table 2 along with the void swelling as determined from measurements of cavity density and mean size. Examples of the cavities at each position are shown in Fig. 6 along with size distributions and densities for the 25- and 55-mm positions in Fig. 7. The cavities in the 1-mm position, which

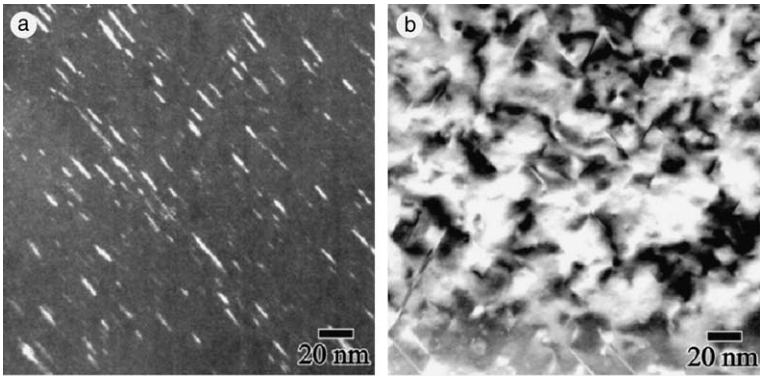

Fig. 2. Frank loops imaged using their rel rods near a $\mathbf{g} = 113$ 2-beam condition are shown in (a). A bright field image obtained near a $\mathbf{g} = 200$ 2-beam conditions is shown in (b), illustrating the complex strain fields that result.

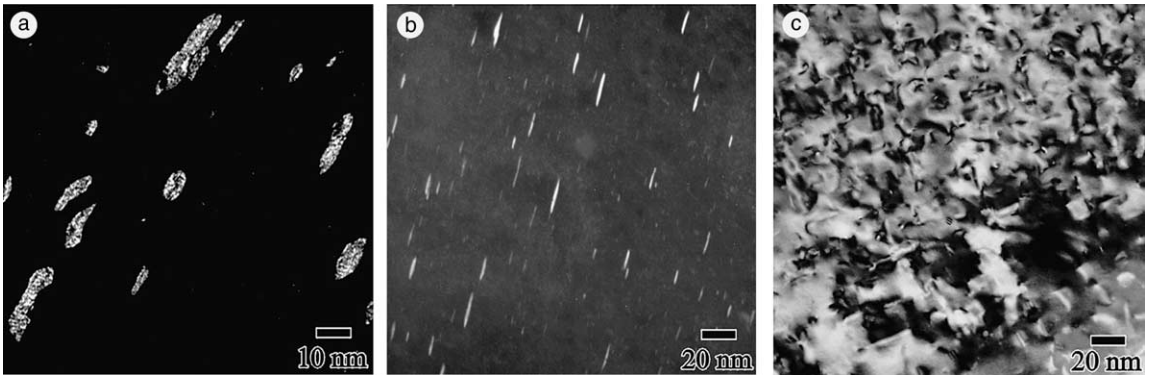

Fig. 3. Rel-rod images of the Frank loops from the 25-mm position are shown inclined in (a) and on edge in (b). A dark field image using a $\mathbf{g} = 200$ 2-beam conditions gives the complex image in (c).

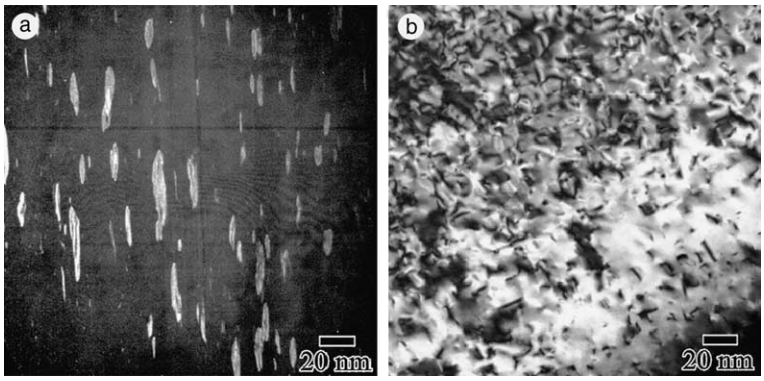

Fig. 4. Rel-rod images of slightly inclined Frank loops are shown in (a) along with a matrix dark field image in (b) using a $\mathbf{g} = 200$ 2-beam condition. The bright field does not allow clear imaging of the individual loops in a manner that allows for their quantification.

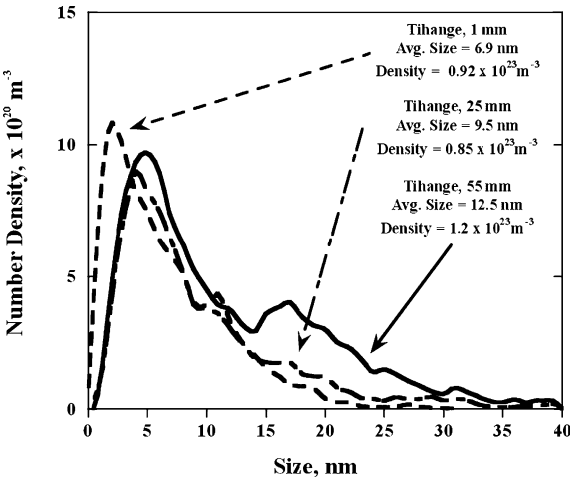

Fig. 5. Size distributions are shown for the Frank loops observed in each position. All size distributions are asymmetric, and there is evidence of a second peak in the distribution of loops from the 55-mm position.

might be either bubbles or very small voids, were not distributed homogenously throughout the grain interiors. Many areas were completely free of cavities whereas other areas tended to have loose clusters of cavities. The small number of cavities at the 1-mm position did not allow any size distributions with meaningful statistics to be obtained. Note that many of the cavities at the 25- and 55-mm positions were typically faceted in appearance, which identifies them as voids as opposed to pressurized He bubbles. The cavities stood out in strong contrast because of the Fresnel fringes around the edge of the void or bubble. According to Jenkins and Kirk [12], for cavities over 5 nm in diameter it is best to measure the diameter from the center of the dark Fresnel fringe on each side of the cavity. Cavities smaller than 5 nm become more difficult to measure accurately, and in fact below 2 nm they cannot be sized accurately from TEM images. All measurements of the diameter of the cavities were taken from images near the $\langle 0\,1\,1 \rangle$ zone axis along the $\mathbf{g} = 200$ condition, but tilted to a kinematical condition.

Fine-scale precipitation was found to be present in the shank positions and tentatively in the 1-mm bolt head position. At the shank positions it was confirmed that γ' precipitates existed on a very fine scale, appearing to form on the pre-existing dislocation network, as reported by Gelles [13] at higher irradiation temperatures. Examples of the γ' precipitates found at the 25-mm position are shown in Fig. 8(a) with the associated diffraction pattern (Fig. 8(c)). The γ' precipitates were present in a density of $\sim 0.6 \times 10^{23}$ m^{-3} with an average size of $\sim$3 nm. An additional precipitate phase was observed in the microstructure (Fig. 8(b)) at a lower den-

Table 2
Density and average sizes of loops and cavities for each position

Position (mm)	Dose (dpa)	Irradiation temperature (°C)	Frank loops		Cavities		Swelling (%)
			Density ($\times 10^{23}$ m^{-3})	Average size (nm)	Density ($\times 10^{22}$ m^{-3})	Average size (nm)	
1	19.5	320	0.92	6.9	$<10^{20}$	<2	<0.01
25	12.2	343	0.85	9.5	0.61	8.6	0.20
55	7.5	333	1.2	12.5	1.0	7.7	0.24

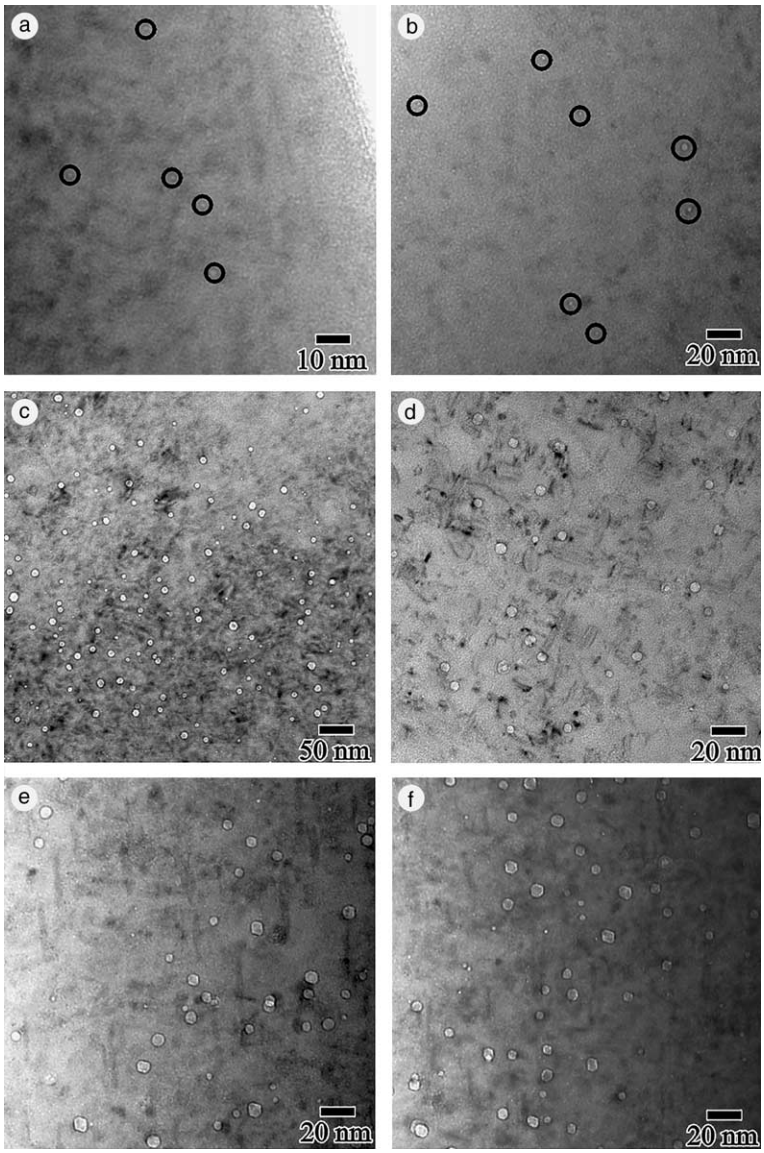

Fig. 6. Examples are shown in (a) and (b) of the small cavities (encircled) present in a low density in the 1-mm bolt head position. Larger cavities are present at the 25-mm position as shown in (c) and (d), and at the 55-mm position as shown in (e) and (f). The level of swelling in the bolt head was estimated to be less than 0.01%, and up to ~0.2% in the two shank positions.

sity of $\sim 0.2 \times 10^{23}$ m^{-3} with a larger average size of ~8.5 nm. The extra reflections present in the diffraction pattern shown in Fig. 8(d) could not be matched conclusively with any particular phase. Neither type of precipitate was observed to coincide with either the voids or the Frank loops.

3.2. Grain boundary microchemical characterization

3.2.1. 25-mm position (12.2 dpa, 616 K)

Compositional profiles for two grain boundaries are presented in Fig. 9. Both grain boundaries were depleted in Cr and Fe, while enriched in Ni and Si. The profile shapes reveal that the radiation-induced segregation (RIS) width was approximately ±6 nm for most elements except Cr, which is slightly wider. Grain boundary #1 exhibited larger levels of segregation compared to the other grain boundary. Both grain boundaries were depleted to levels of ~10–12%, but the Cr profile in Fig. 9(a) indicates additional structure, with a secondary minima at 15% Cr approximately 4 nm from the boundary. The Fe was depleted at the boundaries by 10–12 wt%, with evidence of a slight enrichment ~4 nm from the boundary. The Ni composition exhibited the

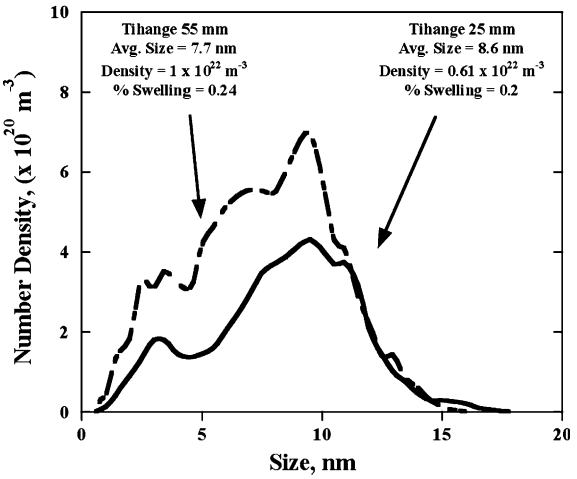

Fig. 7. Size distributions for the cavities in the 25- and the 55-mm position are shown. The small peak at ~4 nm may be remnants of the He-bubbles.

greatest change, enriching at the boundary to levels 24–27 wt%, more than double the average matrix composition of 11 wt% Ni. Silicon reached levels of ~4.5 wt% at boundaries in comparison to less than ~1 wt% in the matrix. Molybdenum was depleted at grain boundaries, but considerable scatter was observed in the measurements. Minimum interfacial Mo levels ranged from 0.6 to 1 wt% versus measured matrix concentrations of ~2.2 wt%. Phosphorus was detected in a few grain boundary analyses, but only at trace levels.

3.2.2. 55-mm position (7.5 dpa, 606 K)

Compositional profiles from two high-energy grain boundaries in the 55-mm position sample are presented in Fig. 10. Each boundary was depleted in Fe and Cr and enriched in Ni, but to different degrees. Grain boundary #1 showed very little Fe depletion and a small amount of Cr depletion. The second grain boundary exhibited a more clearly defined depletion profile for both elements. The largest difference between the two boundaries was for Fe with significant depletion in boundary #2 (~6%) and essentially no depletion in boundary #1. As in the case of the boundaries from the 25-mm position, there was a slight enrichment of Fe and perhaps Cr in the 6-nm regions adjacent to the boundaries. Nickel was enriched to higher levels in the second grain boundary, reaching a peak at ~21% compared to ~16% Ni for the first grain boundary. There was also a slight depletion in Ni immediately to either side of the boundaries.

Attempts to quantify Si and Mo concentrations at or near grain boundaries in this sample were not suc-

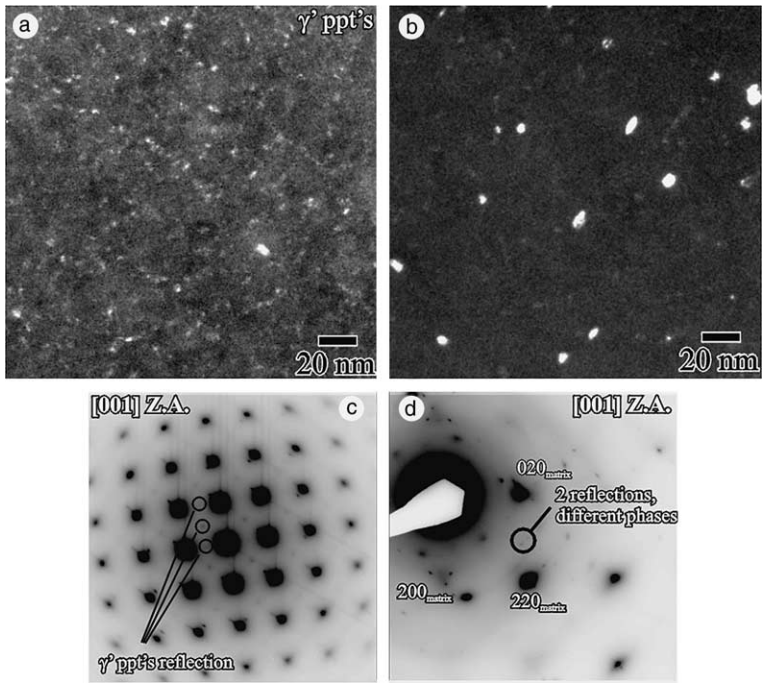

Fig. 8. Precipitates of the γ' phase are shown in (a), while the dark field image in (b) shows precipitates of an unidentified phase. The cube-on-cube orientation relationship between the γ' phase and the austenitic matrix is shown in the diffraction pattern given in (c). The diffraction patterns in (d) show the extra reflection used to image the small, unidentified phase in (a).

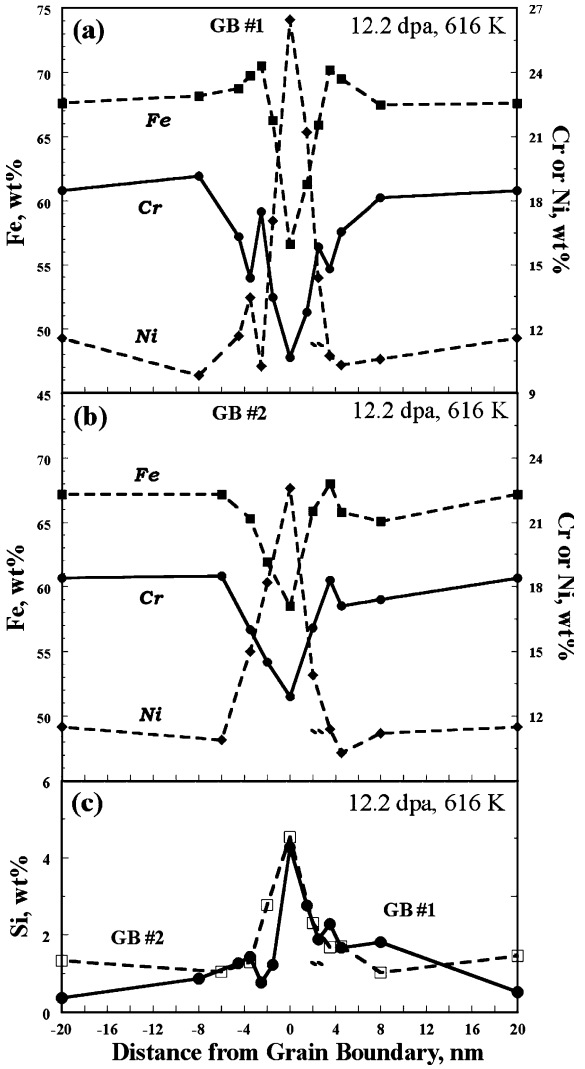

Fig. 9. Profiles of two grain boundaries from the 25-mm position are provided illustrating the depletion of Fe and Cr from both boundaries while Ni and Si are enriched.

cessful. Slight Si enrichment was found in all areas, probably arising from insufficient rinsing following electropolishing. Measurements did indicate some Si enrichment at grain boundaries (up to ~2 wt%) above that in the matrix. Considerable scatter was again observed in the Mo concentrations and conclusive evidence of grain boundary depletion could not be established for these two boundaries. Because of these problems with Si and Mo, neither of these elements was included in the analyses for the major alloying elements. Several additional samples were prepared from the 55-mm position to improve on the data set, but none contained adequate boundaries for high-resolution EDS analysis.

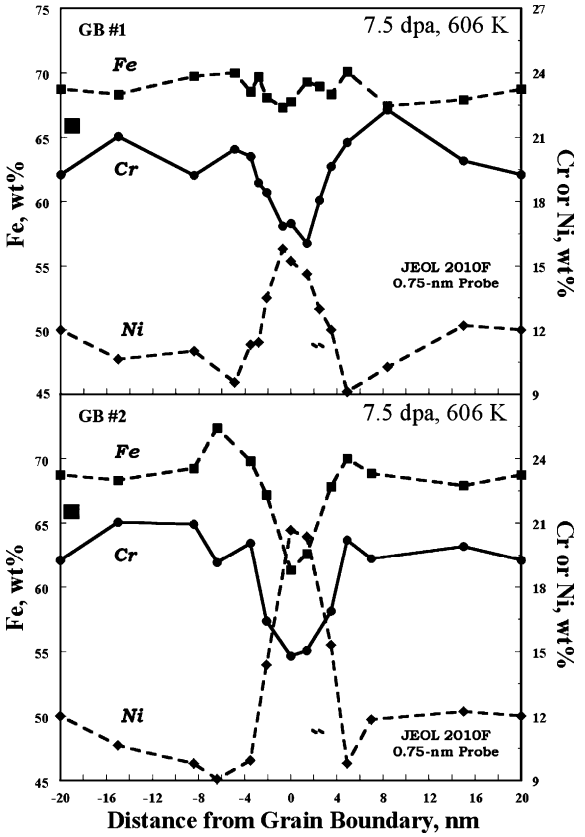

Fig. 10. Profiles of two grain boundaries from the 55-mm position are provided illustrating the depletion of Fe and Cr and the enrichment of Ni at both boundaries.

3.3. Composition at void surfaces

A check was made of the segregation to the void surfaces at the 25-mm position. The void surfaces were depleted in Fe and Cr and enriched in Ni. Chromium was found to be consistently depleted whereas the Ni was enriched to levels well above matrix levels. The measured Si and Mo concentrations where too variable to draw any firm conclusions, but there did appear to be an indication of enrichment of Si at the void surfaces. For example, a void surface with 19.5% Ni also included ~3 wt% Si. It is possible that the degree of segregation depends on the size of the void, leading to the variability observed in the RIS measurements.

3.4. Hardness testing

Hardness testing at room temperature revealed average hardness levels of 378, 355, and 366 kg/mm^2 at the 1-, 25- and 55-mm positions, respectively. The bolt head position, which contains a distribution of smaller Frank

Table 3
Helium and hydrogen concentrations in the Tihange baffle bolt 2K1R5

Position (mm)	^{1}H (appm)	^{4}He (appm)
1	493, 743	71
25	720, 1260, 3660, 3710	52.7
55	1840, 3740	48.8

loops and cavities, is therefore the hardest compared to the shank positions.

3.5. Helium and hydrogen measurements

The helium and hydrogen measurements for each position are summarized in Table 3. The bolt head contains the highest level of helium at 71 appm, whereas the 25- and 55-mm positions contain roughly 50 appm He. The low density of cavities in the bolt head position indicates that much of the helium is still in solid solution or in very fine, unresolvable cavities. On the other hand, the higher irradiation temperature at the 25- and 55-mm positions leads to the formation of voids and possibly a smaller distribution of helium bubbles.

The 25- and 55-mm positions contain concentrations of hydrogen 3–7 times higher than that measured at the 1-mm position. Variations in the hydrogen levels existed not only along the length of the bolt, but also from specimen to specimen taken from each position.

4. Discussion

4.1. Evolution of loops and cavities

Much of the literature regarding IASCC phenomenon in austenitic stainless steels pertains to irradiation temperatures below ~573 K. This temperature represents annealing stage V, above which vacancy clusters and loops begin to lose their thermal stability and emit vacancies into the lattice [14]. Below this temperature the microstructure is composed primarily of small dislocation loops and clusters of vacancies and interstitials.

Recent work by Edwards et al. [7,8] demonstrated that the small, visible defects that form in commercial austenitic stainless steels irradiated at 560 K are primarily Frank loops (faulted dislocation loops that lie on the {1 1 1} planes) and partially-dissociated Frank loops, both of which extended down to sizes less than 1 nm, a size regime normally described as 'black spot' damage. Other defects such as vacancy-type stacking fault tetrahedra were observed only in high purity 304 and 316SS, but these comprised just a few percent of the total defect population. Based on the fact that the Frank loops were the dominant defect, Edwards and coworkers [7,8] concluded that the visible loops at this irradiation temperature were likely both vacancy- and interstitial-type Frank loops. However, the details of how each population evolved relative to each other and as a function of neutron dose remains unclear. This conclusion differs from the literature in the sense that many researchers considered Frank loops to be strictly interstitial-type loops, and the vacancies tied up separately in black spots defects that are distinct from the Frank loop microstructure. The presence of both vacancy- and interstitial-type Frank loops is important given that the stability of the two types of loops will likely be different as a function of irradiation temperature and loop size. The most convincing evidence of this follows from the observation that at higher irradiation temperatures ($T_{irr} > 673$ K), only interstitial-type Frank loops are observed and the vacancies are partitioned into cavities [14–16]. The import of this difference in loop stability is related to the fact that the Tihange bolt was irradiated at a temperature above which vacancy-type loops are normally considered to lose their stability.

As the irradiation temperature is raised above ~573 K, additional defect types begin to evolve due to a change in the stability of the vacancy-type defects. The vacancy-type Frank loops and clusters do not survive long enough to grow to large sizes, instead they dissociate and emit vacancies into the lattice. Interstitial-type Frank loops remain stable up to much higher temperatures, and therefore can continue to grow depending on the relative flux of interstitials and vacancies. The release of the vacancies from previously stable clusters increases the vacancy concentration, leading to the nucleation and growth of gas-stabilized cavities, namely He bubbles and voids. Void formation is extremely sensitive to the irradiation temperature, dose rate, and He production rate, as well as microstructural variables such as material composition, prior cold work level and the presence of second phases [15]. Although no evidence of voids has ever been reported for irradiation temperatures below ~573 K in austenitic stainless steels, Maziasz [16] and Zinkle et al. [14] did report that a high density of ultrafine He bubbles was observed at irradiation temperatures below 573 K. Porollo and coworkers [17,18] have shown that there appears to be a lower temperature limit of ~578 K for void formation at PWR-relevant displacement rates in the Russian equivalent of AISI 321SS, even at doses approaching 56 dpa.

In the Tihange bolt, the irradiation temperature is always above the critical temperature throughout the length of the bolt, leading to a microstructure composed of cavities in addition to the Frank loops. As described earlier, the microstructure exhibits different characteristics depending on the location along the length of the bolt. From this study is not possible to derive the relative importance of gradients in the dose rate versus the irradiation temperature. The influence of dose rate versus temperature may be difficult to discern since the loop

microstructure has reached such a saturated state that the differences become minimal above a certain dose. It seems likely, particularly given the differences in the cavity microstructure along the bolt, that irradiation temperature plays the larger role since it can affect the stability of the vacancy-type defects so strongly as well as the overall kinetics. While dose rate changes may affect the details of the Frank loop and cavity evolution, this will be masked by the changes in the irradiation temperature along the length of the bolt as well as during the individual irradiation cycles.

Edwards et al. [7,8] presented size distributions for Frank loops obtained from a solution annealed 316SS (labeled 316-K) irradiated in the core of a BWR at ~560 K at a displacement rate considerably higher (approximately a factor 10 higher) than in the case of this bolt. The Frank loop microstructure was imaged in the same manner as in this study, providing a useful comparison with the data presented here. The size distributions for the shank positions of the Tihange bolt are compared in Fig. 11 to that measured for the 316-K irradiated to 5.7 and 13.3 dpa. The most noticeable difference is that the loop size distributions extend to larger sizes (40 versus 20 nm) in the Tihange bolt shank compared to the loops in the 316-K. The densities appear to be lower in the bolt shank positions, though these differences are close to being within the factor of two experimental error. Comparing the size distributions from the 1-mm position and 316-K at 13.3 dpa in Fig. 12 presents a different case. The average size of the loops is smaller and slightly lower in density in the bolt head than in the 316-K, in addition the density peaks at a smaller size than in the 316-K.

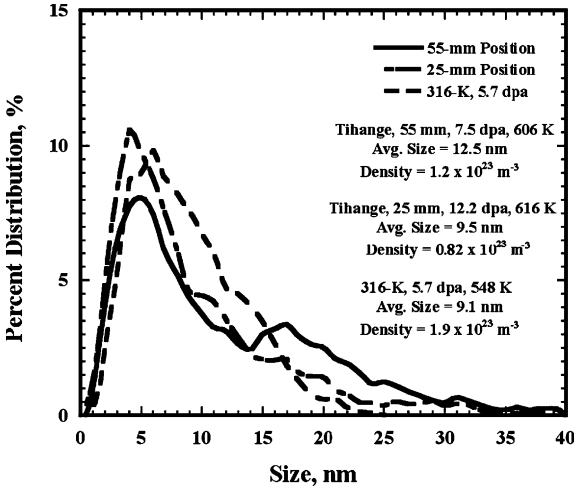

Fig. 11. The size distributions for loops in the 25- and 55-mm position are compared to loops from 316-K irradiated at 560 K to 5.7 dpa [7,8]. Despite the higher irradiation temperatures and doses in the bolt shank positions, there are only subtle differences in the loop distributions.

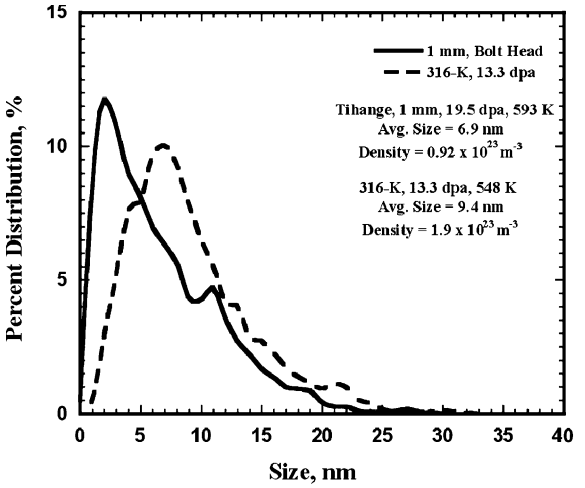

Fig. 12. The size distributions for loops in the 1-mm position are compared to loops from 316-K irradiated at 560 K to 13.3 dpa [7,8]. The loop microstructure shows a small average size and lower density than found in the 316SS irradiated at 560 K. The size distribution of loops in the bolt head position peak at a smaller size than found in the 316-K. The differences may be due to the fact that the bolt was in a cold work condition prior to irradiation.

A comparison of the differences between the Tihange bolt and the 316-K is complicated by the fact that the Tihange bolt was irradiated in a cold-worked condition. As shown previously [14–16], the dense dislocation structure introduced by cold-working can slow the microstructural evolution under irradiation because of the high sink strength for the radiation-produced defects. Recovery of the dislocation structure occurs during irradiation, but this recovery is dependent on irradiation dose and temperature. The lower temperature at the bolt head may have slowed the recovery of the cold-worked dislocation structure, which coupled with the slower kinetics for vacancy emission and the different displacement rate, may be responsible for the finer-scale microstructure found in the bolt head compared to the bolt-shank positions.

The different sensitivity of the cavities and loops to the irradiation conditions is further illustrated by comparing these results with those obtained by Pironet and coworkers [4] on a different bolt. The bolt Pironet et al. characterized had a lower dose (same irradiation time, lower displacement rate) than the bolt examined in this study, and they limited their characterization to the bolt head. While their observations revealed no evidence of cavities, the loops exhibited a size range and density comparable to that measured in this study for the bolt head. This may change as the dose continues to increase and void swelling and precipitation begin to occur.

Irradiation to higher doses may eventually lead to more discernible differences over the temperature range of ~560 to ~673 K as void growth, loop unfaulting and precipitation begin to change the sink strengths and stability of various microstructural features.

A final point to consider is that the irradiation temperature does in fact change during a given reactor cycle due to changing boron levels in the coolant water. The maximum in the temperature fluctuation is near the end of the reactor cycle and is estimated to produce a temperature at the 25-mm position as high as ~623 K. This fluctuation in temperature may lead to changes in the microstructure not accounted for if simply considering a constant irradiation temperature. Given that the bolt is being irradiated in the sensitive temperature regime just above the threshold for swelling, periodic fluctuations in the irradiation temperature may alter the nucleation and growth of cavities and precipitates, and eventually lead to changes in the loop microstructure not predicted based on constant temperature irradiation experiments.

The observation of measurable swelling in this bolt raises a potential concern in that the cold-worked 316SS bolts are surrounded by annealed 304SS former and baffle plates. Considerable research has demonstrated that annealed 304SS has a much shorter incubation period for swelling than cold worked 316SS [14]. Based on this, Garner and coworkers [19–21] predicted that the 304SS in PWR baffle-former assemblies may swell to significant levels in certain positions where the gamma heating leads to high enough temperatures. This swelling will be accelerated by the lower displacement rate, as recently shown by Garner [22], Bond et al. [23] and Okita and coworkers [24,25]. The variation in irradiation temperature during a given irradiation cycle may further alter the swelling characteristics and overall microstructural evolution.

4.2. Radiation-induced segregation and precipitation

Radiation-induced depletion of Cr and Fe occurs at the grain boundaries and void surfaces in the baffle-bolt samples along with Ni and Si enrichment. This segregation behavior is generally consistent with the well-documented RIS results after LWR irradiations at 560–563 K [1]. As noted above, Mo is also depleted at the boundaries (down to ~0.6 wt%) and Si enriched (up to ~4.5 wt%) in the baffle bolt samples. Even though quantitative measurements could not be made at both positions, general indications from the 25-mm results suggest that the RIS of these minor alloying elements is consistent with that seen after LWR irradiations at 560–563 K in similar steels. There appears to be no single variable that dominates grain boundary RIS as a function of position in the baffle bolt. Rather the variations in local irradiation conditions are small enough and tend to be of opposite influence that the net effect on RIS is relatively small. The RIS at void surfaces will likely continue to change if the cavities grow larger and/or increase in density as the doses increases. Although not measured in this study, RIS of Ni and Si to Frank loops was found earlier by Kenik and Hojou [26] and more recently by Edwards et al. [8], so RIS likely occurs to the finely dispersed Frank loops as well.

The γ' precipitation and the evidence for a possible additional precipitate phase indicate that phase instabilities do exist at these irradiation temperatures, which was unexpected since most of the published work indicates precipitation is non-existent at temperatures <623 K [1,14–16]. Hashimoto et al. [27] recently provided evidence of precipitation in 316SS irradiated with neutrons at 333 and 573 K, but the precipitates were tentatively identified as small carbides, not the γ' observed in this study. Bond and coworkers found that fine $M_{23}C_6$ carbides form in annealed 304SS when irradiated at PWR-relevant dose rates and temperatures [23]. The identity of the second precipitate phase may be some type of carbide, but further work is needed to clarify the fine-scale precipitation that occurs in the different positions along the bolt. Precipitation could alter the rate of microstructural evolution and swelling rate, as well as lead to a further decrease in the ductility and toughness. The apparent segregation at the void surfaces and perhaps the Frank loops raises another issue for concern since removal of enough nickel and silicon can alter the phase stability of the base metal.

4.3. Radiation hardening

The measured hardness from 355–378 kg/mm^2 was roughly constant over the length of the bolt up to 55 mm, which correlates well to the observation that the loop microstructure does not vary significantly. Given their size and density, it is thought that the cavities are not significant from a hardening standpoint, however, the precipitation may contribute to some degree and cannot be discounted until it is better characterized and understood. The hardness levels in this bolt were fairly close to that reported earlier by Pironet [4] for the bolt head of Tihange bolt 1E1R1. For the 1-mm position they reported an average hardness level of 410 kg/mm^2, with lower average hardness levels of 340 and 325 kg/mm^2 for the 25- and 55-mm positions, respectively. Although they observed a scatter of ± 25 kg/mm^2 over the length of the bolt, the general trend was that the hardness decreased from the bolt head to the shank positions. The hardness results further support the idea that for the dose range in this bolt, the loop microstructure is in a saturated state and there are no significant differences over the length of the bolt.

The hardness of the Tihange bolt head is similar to that of the 316-K at ~6 dpa reported by Edwards et al.

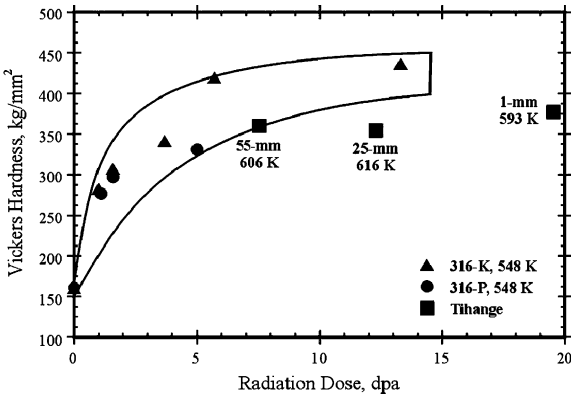

Fig. 13. Room temperature hardness data show no substantial differences over the length of the bolt. Compared to the two 316SS irradiated at 560 K (316-K and 316-P), the bolt is slightly lower in hardness for a comparable dose.

[7,8]. The differences along the length of the bolt are minor in comparison to each other, but are generally lower than that measured for the 316-K for a comparable dose. This is illustrated in Fig. 13, showing a comparison of the room temperature hardness at each position along with the hardness data obtained from the 316SS heats (316-P is similar to the 316-K and is described in references [7,8]). The hardness results appear to agree qualitatively with the longstanding premise that loops control the strength in the material, so therefore the lower hardness in the Tihange bolt is a consequence of the lower density of similar sized loops compared to the Frank loop microstructure in the 316-K at comparable doses.

4.4. Helium and hydrogen

For the Tihange bolt, the thermal flux variation over the length of the bolt can explain the differences in helium concentrations at the different positions within the bolt. To understand this, predictions of the He-generation rate were made based on the fast and thermal neutron spectrum for a typical bolt in the Sizewell B reactor, a reactor of similar design. As shown in Fig. 14, the predictions show that simply altering the thermal flux by factors of 0.85, 1.1 and 1.6 reproduces the helium levels in a consistent manner for the three positions within the bolt. Because of the variation in thermal-to-fast neutron spectrum along the length of the bolt, each data point lies on a separate and non-linear curve through the origin as illustrated in Fig. 15. The higher He-generation rates at the lower dpa levels signals that the thermal-to-fast ratio is higher at these positions, thereby increasing the He/dpa ratio. In addition, it can be deduced from such agreement that the original boron content (unknown) of the steel was less than 5 appm. These predictions also demonstrate that the hydrogen content is too large to have been generated strictly by transmutation reactions, which produce at most a few hundred ppm of hydrogen for the doses experienced by the Tihange bolt. Rather the hydrogen is the result of exposure to the PWR coolant and the transmutation reactions are a negligible contributor.

The retention of so much hydrogen raise two issues that bear further study. It has been proposed [28] that He-nucleated cavities and voids in general may allow the storage of hydrogen at LWR-relevant temperatures, although the mechanism is not yet understood. As shown earlier, ~0.2% swelling exists in the 25- and 55-mm

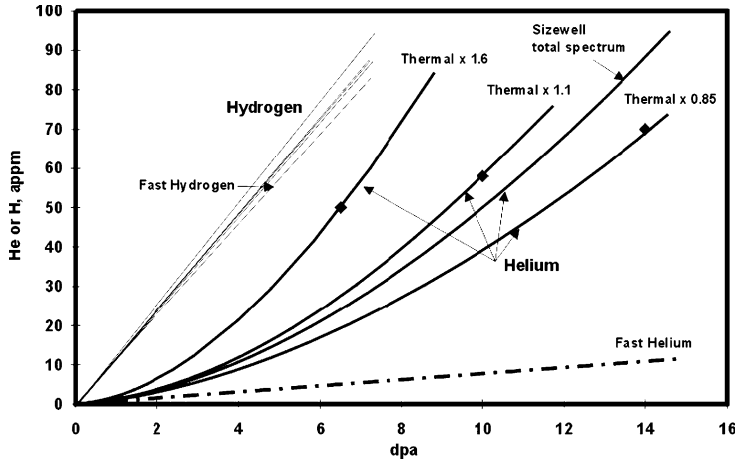

Fig. 14. Changes in the thermal-to-fast ratio over the length of the bolt lead to significant differences in the He/dpa rate. The calculated levels of H formed by the transmutation are relatively small compared to the several thousand appm measured in the shank positions. The thermal-to-fast neutron ratio has little effect on H production.

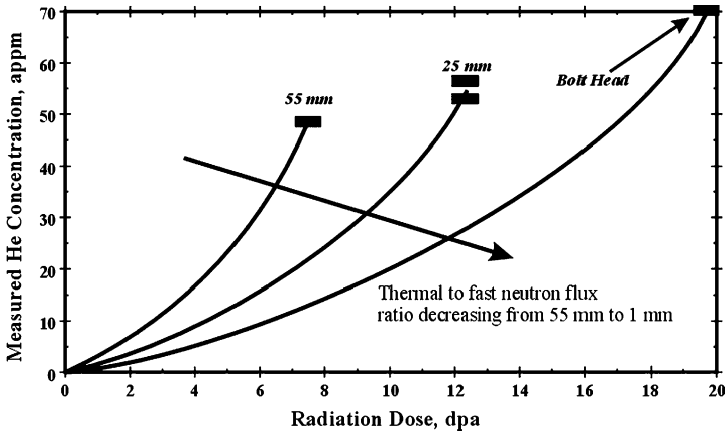

Fig. 15. The He generation rate lies on separate curves for each position due to the differences in thermal-to-fast neutron ratio.

positions where the hydrogen content is highest, but in the bolt head where much less swelling exists there is significantly less hydrogen. The 316 and 304SS irradiated at 560 K [7,8] contained no discernible cavity structure (bubbles or voids) and showed no retention of hydrogen that could be measured above background levels, lending support to the idea that the cavities in the shank positions are effective at storing hydrogen in some form. It is not clear what role, if any, the hydrogen retention has on void nucleation or growth. The other issue is the relatively large range of hydrogen levels for repeated measurements at the same position on the bolt. The origin of this variability has not yet been identified, but may be a consequence of either an inherent local variability in the microstructure or possibly that the hydrogen generation and retention rates are dependent on the radial position within the sample. No attempt was made to maintain a record of where the individual samples were located on the slice taken across the bolt.

5. Summary and conclusions

The characterization reveals that the cavity and loop components of the microstructure exhibit a different sensitivity to the varying irradiation conditions along the length of the bolt. The loop microstructure is a less sensitive indicator of changes in the irradiation conditions along the length of the bolt, exhibiting rather minor variations among the three different positions characterized. The cavities, however, show a noticeable difference in that measurable void swelling exists in the higher temperature shank regions, whereas only small bubbles in a low density are present in the cooler bolt head region. This temperature and dose dependence of the cavity microstructure indicates that a better understanding is needed of the growth and stability of vacancy versus interstitial-type loops, the cavities that eventually form, and ultimately how their interaction affects swelling and microstructural evolution.

One of the more striking consequences of the void swelling is that the shank regions appear to be very effective in retaining hydrogen from the environment, though the mechanism for this remains unclear. The levels of segregation and depletion due to RIS were similar to levels measured at 560 K for other 316 and 304SS, possibly due to the competing effects of higher irradiation temperature and lower dose rate in the bolt. The onset of precipitation was identified in the bolt, but further work is needed to fully understand the precipitation and their influence on swelling, hardening and RIS. The hardening levels across the bolt revealed no substantial differences, and are thought to be mostly related to the loop microstructure with some contribution for the precipitation.

The observation of cavities in 316SS at temperatures and doses relevant for LWR conditions has important implications. While the degree of swelling at these doses remains low, the life extension plans for current operating reactors does raise the issue that the swelling may become more important at higher doses. In addition, the fact that a CW316SS bolt can swell at the doses and dose rates that apply to this component illustrates that the surrounding SA304SS plate may have more significant swelling due to its known shorter incubation period.

Acknowledgements

The assistance of P.M. Scott and R. Gerard is gratefully acknowledged in supplying critical information concerning the baffle-bolt irradiation conditions. Contributions of B.W. Arey for SEM examinations are recognized. Discussions with Larry Thomas are greatly

appreciated for his insights in radiation-induced microstructures and their characterization. Support for this research came from the internationally sponsored Cooperative IASCC Research Program managed by EPRI and from the Materials Sciences Branch of the Office of Basic Energy Sciences, US Department of Energy under contract DE-AC06-76RLO 1830 with Battelle Memorial Institute.

References

[1] S.M. Bruemmer, E.P. Simonen, P.M. Scott, P.L. Andresen, G.S. Was, J.L. Nelson, J. Nucl. Mater. 274 (1999) 299.
[2] R. Cauvin, O. Goltrant, Y. Rouillon, E. Verzaux, A. Cazus, P. Dubuisson, P. Poitrenaud, S. Bellet, Proc. International Symposium Fontevraud III, Société Française d'Energie Nucléaire, 1994, p. 54.
[3] Trenty, D. Deydier, Proc. IAEA Specialists Meeting on Behaviour of Core Materials, Rez, Czech Republic, 6–8 October 1998.
[4] G. Pironet, A. Heuzé, O. Goltrant, R. Cauvin, Proc. International Symposium Fontevraud IV, Société Française d'Energie Nucléaire, 1998, p. 195.
[5] P.M. Scott, M.C. Meunier, D. Deydier, S. Silvestre, A. Trenty, in: R.D. Kane (Ed.), Environmentally Assisted Cracking: Predictive Methods for Risk Assessment and Evaluation of Materials Equipment and Structures, ASTM 1401, American Society for Testing and Materials, West Conshohocken, PA, 2000, p. 21.
[6] D.J. Edwards, F.A. Garner, B.A. Oliver, S.M. Bruemmer, in: S.M. Bruemmer, P. Ford, G. Was (Eds.), 10th International Symposium on Environmental Degradation of Materials in Nuclear Power Systems – Water Reactors, The Minerals, Metals and Materials Society, Pennsylvania.
[7] D.J. Edwards, E.P. Simonen, S.M. Bruemmer, Microstructural Processes in Irradiated Materials, in: G.E. Lucas, L.L. Snead, M.A. Kirk, R.G. Elliman (Eds.), Materials Research Society Symposium, vol. 650, 2000, p. R2.7.
[8] D.J. Edwards, E.P. Simonen, S.M. Bruemmer, J. Nucl. Mater. 317 (2003) 13.
[9] F.A. Garner, D.J. Edwards, B.M. Oliver, L.R. Greenwood, P. Scott, R. Gerard, Proceedings of the 21st ASTM International Symposium on Radiation Effects in Materials, 2002, in press.
[10] H. Farrar, B.M. Oliver, J. Vacuum Sci. Technol. A 4 (1986) 1740.
[11] B.M. Oliver, F.A. Garner, L.R. Greenwood, J. Nucl. Mater. 283–287 (2000) 1006.
[12] M.L. Jenkins, M.A. Kirk, Characterization of Radiation Damage by Transmission Electron Microscopy Institute of Physics, IOP, London, 2000.
[13] D.S. Gelles, The Metal Science of Stainless Steel, in: E.W. Collings, H.W. King (Eds.), American Institute of Mining Metallurgy and Petroleum Engineers Inc., 1979, p. 130.
[14] S.J. Zinkle, P. Maziasz, R.E. Stoller, J. Nucl. Mater. 206 (1993) 266.
[15] F.A. Garner, in: Chapter 6: Irradiation Performance of Cladding and Structural Steels in Liquid Metal Reactors, Materials Science and Technology: A Comprehensive Treatment, vol. 10A, VCH Publishers, 1994, p. 419.
[16] P. Maziasz, J. Nucl. Mater. 205 (1993) 118.
[17] S.I. Porollo, Y.V. Konobeev, A.M. Dvoraishin, V.M. Krigan, F.A. Garner, in: S.M. Bruemmer, P. Ford, G. Was (Eds.), 10th International Symposium on Environmental Degradation of Materials in Nuclear Power Systems-Water Reactors, The Minerals, Metals and Materials Society, Pennsylvania, 2001.
[18] S.I. Porollo, Y.V. Konobeev, A.M. Dvoraishin, V.M. Krigan, F.A. Garner, Proceedings of the 10th International Conference on Fusion Reactor Materials, held in Baden-Baden, Germany, October 2001.
[19] F.A. Garner, Materials issues involving austenitic pressure vessel internals arising from void swelling and irradiation creep, Trans. Am. Nucl. Soc. 71 (1994) 190.
[20] F.A. Garner, L.R. Greenwood, D.L. Harrod, Proc. Sixth Intern. Symp. on Environmental Degradation of Materials in Nuclear Power Systems – Water Reactors, San Diego, CA, 1–5 August 1993, p. 783.
[21] F.A. Garner, M.B. Toloczko, J. Nucl. Mater. 251 (1997) 252.
[22] F.A. Garner, M.L. Hamilton, D.L. Porter, T. Allen, T. Tsutsui, M. Nakajima, T. Kido, T. Ishii, G. Bond, B. Sencer, J. Nucl. Mater., in preparation.
[23] G.M. Bond, B.H. Sencer, F.A. Garner, M.L. Hamilton, T.R. Allen, D.L. Porter, in: S.M. Bruemmer, P. Ford, G. Was (Eds.), 9th International Symposium on Environmental Degradation of Materials in Nuclear Power Systems-Water Reactors, The Minerals, Metals and Materials Society, Pennsylvania, 1999, p. 1045.
[24] T. Okita, N. Sekimura, T. Iwai, F.A. Garner, in: S.M. Bruemmer, P. Ford, G. Was (Eds.), 10th International Symposium on Environmental Degradation of Materials in Nuclear Power Systems – Water Reactors, The Minerals, Metals and Materials Society, Pennsylvania, 2001.
[25] T. Okita, N. Sekimura, F.A. Garner, L.R. Greenwood, in: S.M. Bruemmer, P. Ford, G. Was (Eds.), 10th International Symposium on Environmental Degradation of Materials in Nuclear Power Systems-Water Reactors, The Minerals, Metals and Materials Society, Pennsylvania, 2001.
[26] E.A. Kenik, K. Hojou, J. Nucl. Mater. 191–194 (1992) 1331.
[27] N. Hashimoto, E. Wakai, J.P. Robertson, J. Nucl. Mater. 273 (1999) 95.
[28] F.A. Garner, B.M. Oliver, L. R Greenwood, D.J. Edwards, S.M. Bruemmer, M.L. Grossbeck, in: S.M. Bruemmer, P. Ford, G. Was (Eds.), 10th International Symposium on Environmental Degradation of Materials in Nuclear Power Systems – Water Reactors, The Minerals, Metals and Materials Society, Pennsylvania, 2001, in press.